Extraction of nuclear imaginary potential from the excitation function of backward quasi-elastic scattering*

Hui-yan Li (李慧艳)[1] Cheng-jian Lin (林承键)[1,2†] Lei Yang (杨磊)[1‡] Hui-ming Jia (贾会明)[1]
Pei-wei Wen (温培威)[1] Nan-ru Ma (马南茹)[1] Feng Yang (杨峰)[1] Tian-Peng Luo (骆天鹏)[1]
Chang Chang (常昶)[1] Hai-rui Duan (段海锐)[1] Song-xian Zhu (祝颂娴)[1] Cheng Yin (尹诚)[1]
Zhi-jie Huang (黄志杰)[1] Hao-rui Wang (王浩睿)[1] Ze-rui Fan (范泽睿)[1] Ling-yi Fu (傅凌逸)[1]

[1]China Institute of Atomic Energy, Beijing 102413, China
[2]College of Physics and Technology, Guangxi Key Laboratory of Nuclear Physics and Technology, Guangxi Normal University, Guilin 541004,China

Abstract: The nuclear potential is a cornerstone in the study of nuclear structures and reactions. Research on the real part of nuclear potential has been well described using various models; however, that on the imaginary part of nuclear potential remains insufficient. This study proposes a novel method to extract the imaginary nuclear potential from the high-precision excitation function of backward quasi-elastic scattering. The typical systems ^{16}O+^{152,154}Sm, ^{184,186}W with deformed target nuclei were analyzed. Nuclear imaginary potentials were obtained successfully by fitting the excitation functions within the single-channel and coupled-channel frameworks, respectively. A good reproduction at the energy range between sub- and above-barrier energy regions was achieved. Results show long-range imaginary-part potential at a wide energy region covering the Coulomb barrier, consistent with the strong absorption for well-deformed systems. This work is a preliminary attempt to bridge the gap between fusion and scattering and extract the deformation parameters in the whole energy range. The subsequent systematic analysis needs to be further improved.

Keywords: imaginary potential, quasi-elastic scattering, well-deformed nuclei

DOI: 10.1088/1674-1137/adbd18 **CSTR:** 32044.14.ChinesePhysicsC.49064111

I. INTRODUCTION

The nucleus-nucleus interaction potential is a fundamental physical quantity in the study of heavy-ion nuclear reactions, mainly consisting of the repulsive Coulomb potential and absorptive nuclear potential: $U(r) = V_C(r) + V_N(r)$ [1]. The nuclear potential is a crucial component, serving as a construct to account for the many-body interactions between protons and neutrons in the two interacting nuclei that are not explicitly included through channel couplings. Unlike the effective calculation for the Coulomb potential, the nuclear potential has not been well described till now.

A commonly used nuclear potential is the optical-model potential (OMP), written as $V_N(r) = V(r) + \mathrm{i}W(r)$, which consists of an attractive real part and absorptive imaginary part [2]. The optical-potential parameters of the real and imaginary parts have been generally extracted from the analysis of elastic-scattering data [3, 4]. Because of the strong absorption in heavy-ion reactions, the angular distributions for elastic scattering are most sensitive to the tail region of the potential. Therefore, the optical potential extracted from fitting the elastic-scattering angular distribution is not unique, exhibiting Igo ambiguity [5]. To avoid the Igo ambiguity of the optical-potential parameters, the real part of the optical potential can be well calculated using microscopic methods, such as the folding-model potential [6] or proximity potential [7, 8]; however, the imaginary part, such as that obtained by a complex G-matrix [9], is often difficult to satisfy. Therefore, the imaginary part of the phenomenological optical potential is generally used instead.

The optical potential can also be extracted from other reaction channels, such as transfer [10, 11], fusion [12−14], and quasi-elastic scattering [15]. Extracting the optical-potential parameters using the transfer channel

Received 9 January 2025; Accepted 6 March 2025; Published online 7 March 2025

* Supported by the National Key R&D Program of China (2022YFA1602302, 2023YFA1606402, 2024YFE0109804), the National Natural Science Foundation of China (U2167204, 12175313, 12175314, 12235020, 12275360, 12375130), and the Continuous-Support Basic Scientific Research Project

† E-mail: cjlin@ciae.ac.cn

‡ E-mail: yang_lei@ciae.ac.cn

can compensate the shortcomings of the elastic-scattering method, which is insensitive to the low-energy region. However, for systems with obvious coupling effects, the shortcoming calls for a complex coupled-reaction channel (CRC) calculation [10]. For systems with obvious coupling effects, under the incoming-wave boundary condition (IWBC) approximation [16], the real part of the optical potential can be extracted from the fusion data using barrier tunneling [12], but the imaginary part of the nuclear potential is not introduced in this approximation. Notably, the analysis and conclusions obtained through a fusion reaction can only be achieved following the measurement of precise experimental fusion data [17], which is experimentally difficult.

Backward quasi-elastic scattering (QEL) has been shown to be a valuable method to study the nuclear potential, particularly because backward quasi-elastic scattering experimental data are easier and more efficient to measure compared to that of fusion experiments [18]. QEL is defined as the sum of elastic scattering, inelastic scattering, and the nucleon-transfer process. Thus, backward quasi-elastic scattering and fusion are complementary to each other. In general, a short-range imaginary potential with $W = 30$ MeV, $r_{0W} = 1.0$ fm, and $a_W = 0.4$ fm was used to simulate the compound-nucleus formation [19]. Previous studies [20] showed that the calculated results were insensitive to the parameters of the imaginary part of the potential as long as it is strong enough and well localized inside the Coulomb barrier. However, this choice for the parameters of the imaginary part potential is somewhat arbitrary and can not fit the data in the higher-energy region. The fit to the experimental data was not improved, even if the depth, radius and diffuseness parameters of the real-part potential, and deformation parameters were varied [20]. The discrepancy between the experimental data and theoretical calculations for the quasi-elastic excitation function is due to the effect of nuclear distortion with decreasing distance for the two reactants.

To understand nuclear-interaction potentials in the energy region around the Coulomb barrier for the systems ^{16}O with heavy and well-deformed nuclei ^{152,154}Sm and ^{184,186}W, we propose a novel method that extracts the nuclear potential from the high-precision excitation function of backward quasi-elastic scattering. In previous works, the real-part potentials are well described. The parameters may be constrained by requiring that the calculations are consistent with fusion measurements and quasielastic scattering [21, 22]. They may also be taken from systematic parameterizations [7] of fits to elastic-scattering data. However, the description of imaginary potential is insufficient. Therefore, we extract the imaginary-part potential from the backward quasi-elastic excitation function in the case of a fixed real-part potential in this work. The bare potential can be extracted using a coupled-channels (CC) calculation, and the effective potential can be extracted using a single-channel (SC) calculation. Notably, the bare potential extracted here using CC calculation is an empirical bare potential. In practice, all conceivable couplings in the CC calculations cannot be included. For the well-deformed nuclei, the coupling of deformation is explicitly emphasized in the CC calculation. Transfer channels may also play an important role in backward quasi-elastic scattering [23]. Unfortunately, including transfer channels in CC calculations is quite challenging. Therefore, in this paper, we try to incorporate the strong absorption effect within the imaginary potential by adjusting the parameters of the imaginary potential.

The organization of this paper is as follows. We briefly explain the coupled-channels formalism for backward quasi-elastic scattering in Sec. II. The results of the CC and SC calculations are given in Sec. III. We summarize the paper in Sec. IV.

II. COUPLED-CHANNELS FORMALISM FOR BACKWARD QUASI-ELASTIC SCATTERING

This section provides a brief description of the coupled-channel approach (CCFULL [24]) used in the present study. The coupled-channel model CCFULL has been described in detail in Refs. [19, 25].

The total Hamiltonian used in the coupled-channels formalism by considering the intrinsic excitations of the colliding nuclei is given by

$$H = -\frac{\hbar^2}{2\mu}\nabla^2 + V_N^{(0)}(r) + V_C(r) + H_{\rm exct} + V_{\rm coup}(\boldsymbol{r}, \xi_P, \xi_T), \quad (1)$$

where $\boldsymbol{r}$ represents the coordinate for the relative motion between the target and projectile nuclei, μ is the reduced mass, and ξ_T and ξ_P are the coordinate of the intrinsic motion in the target and projectile nuclei, respectively. $V_N^{(0)}$ is the bare nuclear potential. It is assumed to have a Woods-Saxon shape and consists of real and imaginary parts,

$$\begin{aligned} V_N^{(0)}(r) &= V_0(r) - {\rm i}W_0(r) \\ &= \frac{-V_0}{1+\exp[(r-R_0)/a]} + \frac{-{\rm i}W}{1+\exp[(r-R_W)/a_W]}, \end{aligned} \quad (2)$$

where V_0, R_0, and a are the depth, radius, and diffuseness parameters of the real part potential, respectively; W, R_W, and a_W are the depth, radius, and diffuseness parameters of the imaginary part potential, respectively. $V_C(r)$ is the Coulomb potential, given by [26],

$$V_C(r) = \begin{cases} \dfrac{Z_P Z_T e^2}{2R_C}\left(3 - \dfrac{r^2}{R_C^2}\right) & r < R_C \\ \dfrac{Z_P Z_T e^2}{r} & r \geq R_C \end{cases}, \tag{3}$$

where Z_P and Z_T are the projectile and target-charge number, respectively. The Coulomb radius $R_C = r_C(A_T^{1/3} + A_P^{1/3})$ and A_T and A_P are the mass number of the target and projectile nuclei, respectively. $H_{\rm exct}$ describes the excitation spectra of the target and projectile nuclei, whereas $V_{\rm coup}(\boldsymbol{r}, \xi_P, \xi_T)$ is the potential for the coupling between the relative motion and intrinsic excitations of the target and projectile nuclei.

In the iso-centrifugal approximation [24, 27, 28], where the angular momentum of the relative motion in each channel is replaced with the total angular momentum J, the coupled-channels equations derived from the Hamiltonian (1) is obtained as

$$\left[-\frac{\hbar^2}{2\mu}\frac{{\rm d}^2}{{\rm d}r^2} + \frac{J(J+1)\hbar^2}{2\mu r^2} + V_N^{(0)}(r) + V_C(r) - E + \epsilon_n\right] u_n(r) + \sum_m V_{nm} u_m(r) = 0, \tag{4}$$

where ϵ_n is the eigenenergy for the nth channel. $V_{nm}(r)$ are the matrix elements for the coupling potential $V_{\rm coup}$.

The intrinsic coordinates ξ_P and ξ_T in the coupling potential, $V_{\rm coup}$, is replaced with the dynamical operators $\hat{O}_P$ and $\hat{O}_T$. In this way, the coupling potential is given by

$$V_{\rm coup}(r, \hat{O}_P, \hat{O}_T) = V_C(r, \hat{O}_P, \hat{O}_T) + V_N(r, \hat{O}_P, \hat{O}_T), \tag{5}$$

$$V_N(r, \hat{O}_P, \hat{O}_T) = \frac{-V_0}{\left\{1 + \exp\left[\dfrac{r - R_0 - \hat{O}_P - \hat{O}_T}{a}\right]\right\}} + \frac{-{\rm i}W}{\left\{1 + \exp\left[\dfrac{r - R_W - \hat{O}_P - \hat{O}_T}{a_W}\right]\right\}} - V_N^{(0)}(r), \tag{6}$$

In order to avoid double counting, we have subtracted $V_N^{(0)}(r)$ in Eq. (6).

For a deformed target nucleus,

$$\hat{O}_T = \beta_2 R_T Y_{20} + \beta_4 R_T Y_{40} \tag{7}$$

is used for rotational coupling, where the target radius $R_T = r_T A_T^{1/3}$, $Y_{\lambda 0}$ is the spherical harmonics, and β_2 and β_4 are the quadrupole and hexadecapole deformation parameters of the target nucleus, respectively. These deformation parameters quantify the deviation from spherical symmetry and are critical for describing rotational excitations in well-deformed nuclei. The coupling-matrix element between the $|n\rangle = |I0\rangle$ and $|m\rangle = |I'0\rangle$ states of the ground rotational band of the target is given by [25]

$$\hat{O}_{II'} = \sum_{\lambda=2,4} \sqrt{\frac{(2\lambda+1)(2I+1)(2I'+1)}{4\pi}} \beta_\lambda R_T \begin{pmatrix} I' & \lambda & I \\ 0 & 0 & 0 \end{pmatrix}^2, \tag{8}$$

and $\hat{O}$ satisfies

$$\hat{O}|\alpha\rangle = \lambda_\alpha |\alpha\rangle. \tag{9}$$

The nuclear-coupling matrix elements are then evaluated as

$$\begin{aligned} V_{nm}^{(N)} &= \langle n|V_N\left(r, \hat{O}_P, \hat{O}_T\right)|m\rangle - V_N^{(0)}(r)\delta_{n,m}, \\ &= \sum_\alpha \langle n \mid \alpha\rangle\langle \alpha \mid m\rangle V(r, \lambda_\alpha) - V_N^{(0)}(r)\delta_{n,m}. \end{aligned} \tag{10}$$

The last term in this equation is included to avoid the double counting of the diagonal component.

For the Coulomb interaction of the deformed target, the matrix elements are then given by

$$V_{nm}^{(C)} = \begin{cases} \displaystyle\sum_{\lambda=2,4} \eta_\lambda \sqrt{\frac{(2\lambda+1)(2I+1)(2I'+1)}{4\pi}} \begin{pmatrix} I' & \lambda & I \\ 0 & 0 & 0 \end{pmatrix}^2 \frac{Z_P Z_T e^2}{r}\left(\frac{r}{R_T}\right)^\lambda & r \leq R_T \\ \displaystyle\sum_{\lambda=2,4} \eta_\lambda \sqrt{\frac{(2\lambda+1)(2I+1)(2I'+1)}{4\pi}} \begin{pmatrix} I' & \lambda & I \\ 0 & 0 & 0 \end{pmatrix}^2 \frac{Z_P Z_T e^2}{r}\left(\frac{R_T}{r}\right)^\lambda & r > R_T, \end{cases} \tag{11}$$

where

$$\eta_\lambda = \begin{cases} \beta_2 + \dfrac{2}{7}\sqrt{\dfrac{5}{\pi}}\beta_2^2, \lambda = 2 \\ \beta_4 + \dfrac{9}{7}\beta_2^2, \lambda = 4 \end{cases}. \tag{12}$$

The total coupling-matrix element is given by the sum of $V_{nm}^{(N)}$ and $V_{nm}^{(C)}$.

The coupled-channels equations, Eq. (1), are solved with the scattering boundary condition for $u_n(r)$ [19]:

$$u_n(r) \to \frac{i}{2}\left[H_J^{(-)}(k_n r)\delta_{n,n_i} - \sqrt{\frac{k_i}{k_n}} S_n^J H_J^{(+)}(k_n r)\right];\ r \to \infty \quad (13)$$

where S_n^J is the nuclear S-matrix. $H_J^{(-)}(k_n r)$ and $H_J^{(+)}(k_n r)$ are the incoming and outgoing Coulomb wave functions, respectively. The channel wave number k_n is given by $\sqrt{2\mu(E-\epsilon_n)/\hbar^2}$ and $k_i = \sqrt{2\mu E/\hbar^2}$. The scattering angular distribution for the channel n is then given by

$$\frac{d\sigma_n}{d\Omega} = \frac{k_n}{k_i}|f_n(\theta)|^2 \quad (14)$$

with

$$f_n(\theta) = \sum_J e^{i[\sigma_J(E)+\sigma_J(E-\epsilon_n)]}\sqrt{\frac{(2J+1)}{4\pi}} \times Y_{J0}(\theta)\frac{-2i\pi}{\sqrt{k_i k_n}}(S_n^J - \delta_{n,n_i}) + f_C(\theta)\delta_{n,n_i}, \quad (15)$$

where $\sigma_J(E)$ and $f_C(\theta)$ are the the Coulomb phase shift and Coulomb scattering amplitude, respectively. The differential quasi-elastic cross section is then calculated to be

$$\frac{d\sigma^{\rm QEL}}{d\Omega} = \sum_n \frac{d\sigma_n}{d\Omega}. \quad (16)$$

This formalism may be applied to perform a coupled-channels analysis for the backward quasi-elastic scattering of all systems.

III. THEORETICAL CALCULATIONS AND ANALYSIS

In this section, we present the results of our detailed coupled-channels analysis for large-angle quasi-elastic scattering data of ^{16}O+^{152,154}Sm, ^{184,186}W systems. The experiment was performed at the HI-13 tandem accelerator of the China Institute of Atomic Energy. More details can be found in Ref. [15].

The differential cross section for the quasi-elastic events at each beam energy was normalized with a Rutherford scattering cross section. The center-of-mass energy ($E_{\rm c.m.}$) was corrected for centrifugal effects at each angle as follows [23]:

$$E_{\rm eff} = \frac{2E_{\rm c.m.}}{(1+{\rm cosec}(\theta_{\rm c.m.}/2))}. \quad (17)$$

The quasi-elastic barrier distribution $D_{\rm QEL}(E_{\rm eff})$ from the quasi-elastic function was determined using the relation [23]:

$$D_{\rm QEL}(E_{\rm eff}) = -\frac{d}{dE_{\rm eff}}\left[\frac{d\sigma_{\rm QEL}(E_{\rm eff})}{d\sigma_{\rm R}(E_{\rm eff})}\right]. \quad (18)$$

A point difference formula [29] is used to evaluate the barrier distribution, with an energy step $\Delta E_{\rm eff}$ of approximately 2 MeV.

A. Fitting data

The CC and SC calculations were preformed with a modified version of the code CCFULL [24] for quasi-elastic scattering with an energy-independent nuclear potential of Woods-Saxon form. The analysis process involves the following steps:

(1) Initialization of the input radius and coupling parameters;

The radius parameter for the projectile ($r_{\rm P}$) was 1.2 fm in the coupled-channels Hamiltonian. The Coulomb and nuclear parts for both quadrupole and hexadecapole deformations of the target nuclei were kept at the same values. The used Coulomb-radius parameter is r_{0C} = 1.1 fm, which has little influence on the cross section. The coupling parameters of the target nuclei for all the reactions studied here are summarized in Table 1. For the rotational target nuclei, the deformation parameters were taken from [30] with $r_{\rm T}$ = 1.16 fm. In the SC calcultions, when $N_{\rm rot} = 0$, other parameters were consistent with those used in the CC calculations.

Excitations in ^{16}O are not explicitly considered in the calculations, as they simply renormalize the potential due to the large excitation energies [25]. This effect can be included in the potential and will not be considered explicitly in the CC calculations.

(2) Initialization of the real potential parameters (fixed via the Akyüz-Winther potential [7]);

For the real-part potential used in the CC and SC calculations, we use the proximity potential type Akyüz-Winther potential (labeled as AW95) [7], derived from a least-squares fit to experimental elastic-scattering data. A

Table 1. Coupling parameters used in the calculations. E_x denotes the energy of the first excited state (2^+) of the ground-state rotational band [31]. (β_2, β_4) denotes the deformation parameters [30] within the rotational models, respectively. $N_{\rm rot}$ is the number of rotational states considered in the coupled-channels calculations.

Nucleus	E_x /MeV	β_2	β_4	$N_{\rm rot}$
^{152}Sm	0.122	0.237	0.097	5
^{154}Sm	0.082	0.270	0.105	5
^{184}W	0.111	0.232	-0.093	5
^{186}W	0.122	0.221	-0.095	5

previous study [8] showed that the fusion cross sections are well explained by the AW95 potential at energies below as well as above the barrier.

$$V_0(r) = -\frac{V_0}{1+\exp(\frac{r-R_0}{a})}\text{MeV}; \tag{19}$$

$$\text{with } V_0 = 16\pi\frac{R_P R_T}{R_P+R_T}\gamma a, \tag{20}$$

where

$$a = \left[\frac{1}{1.17(1+0.53(A_P^{-1/3}+A_T^{-1/3}))}\right]\text{fm}, \tag{21}$$

$$\gamma = \gamma_0\left[1-k_s\left(\frac{N_P-Z_P}{A_P}\right)\left(\frac{N_T-Z_T}{A_T}\right)\right], \tag{22}$$

where $\gamma_0 = 0.95$ MeV/fm^2, $k_s = 1.8$, and $R_0 = R_P + R_T$. Here, radius R_i has the form

$$R_i = 1.20A_i^{1/3} - 0.09 \text{ fm}. \tag{23}$$

For all the systems, the corresponding parameters of the real potential and uncoupled barrier parameters are listed in Table 2.

(3) Iterative optimization of the imaginary-potential parameters W, r_W, and a_W through a χ^2 minimization procedure, and thus, the value of W, r_W, and a_W giving the best fit to the data.

The parameter optimization was implemented via the popular Minuit minimization program [32], combined with the Differential Evolution (DE) algorithm [33] for a global search in the hypersurface of the χ^2 function. The DE algorithm was first employed to explore the parameter space (W, r_W and a_W) across multiple CPU cores, generating initial guesses near the global minimum. This parallelized approach reduced the computational time compared to traditional grid searches. Subsequently, the Minuit program refined these parameters via gradient-based minimization. This hybrid strategy effectively balanced exploration and exploitation, mitigating the risk of local minimum traps.

For each combination of W, r_W and a_W, the value of χ^2 was calculated between the experimental QEL excitation function and theoretical calculations:

$$\chi^2(W, r_W, a_W) = \sum_{i=1}^{N}\frac{[\sigma_i^{qel} - \sigma_i(W, r_W, a_W)]^2}{\delta\sigma_i^{\,2}}, \tag{24}$$

where $\delta\sigma_i$ is the uncertainty of the data, and $\sigma(W, r_W, a_W)$ represents the CCFULL calculation corresponding to a particular combination of W, r_W and a_W. The χ^2 function (Equation (24)) was minimized to determine the best-fit parameters.

1. ^{152,154}*Sm target nuclei*

Samarium nuclei have long been a popular subject for studying nuclear properties due to their permanent deformation [34–36]. The best-fit results for the CC and SC calculations of the ^{16}O +^{152,154}Sm system are shown in Figure 1 (a) and (b), respectively. The specific values are shown in Table 3. It shows a long-range peculiarity. The table shows that the results using imaginary-part parameters in the CC (solid line) and SC (dash-dot-dotted line) calculations well reproduced the experimental data with the theoretical deformation parameters and real-part nuclear potential. The result using the short-range imaginary-part potential (dashed line) in Ref. [19] already deviates from the experimental data at the energy region near the Coulomb barrier, and the peak position of the barrier distribution is shifted towards the high-energy region.

2. ^{184,186}*W target nuclei*

Tungsten nuclei are of interest because they lie in the region where the deformed rare-earth nuclei begin the transition toward the spherical nuclei near ^{208}Pb. ^{152,154}Sm, ^{184,186}W all have positive β_2 values, but Sm isotopes have positive β_4 values and W isotopes have negative β_4 values for the ground-state rotational band. The comparison between the CC and SC results performed using the imaginary-part potentials obtained from the best fit and experimental data is presented in the Figure 2. Similar to the Sm case, the CC (solid line) and SC (dash-dot-dotted line) calculation results also well reproduce the experimental data for the theoretical deformation para-

Table 2. Real-part potential parameters V_0, r_0, and a using AW95 [7] and corresponding uncoupled-barrier parameters.

System	V_0 /MeV	r_0 /fm	a /fm	V_B /MeV	R_B /fm	$\hbar\omega$ /MeV
^{16}O+^{152}Sm	62.42	1.18	0.65	60.96	10.97	4.42
^{16}O+^{154}Sm	62.53	1.18	0.65	60.79	11.01	4.40
^{16}O+^{184}W	63.99	1.18	0.66	70.55	11.33	4.59
^{16}O+^{186}W	64.07	1.18	0.66	70.38	11.36	4.58

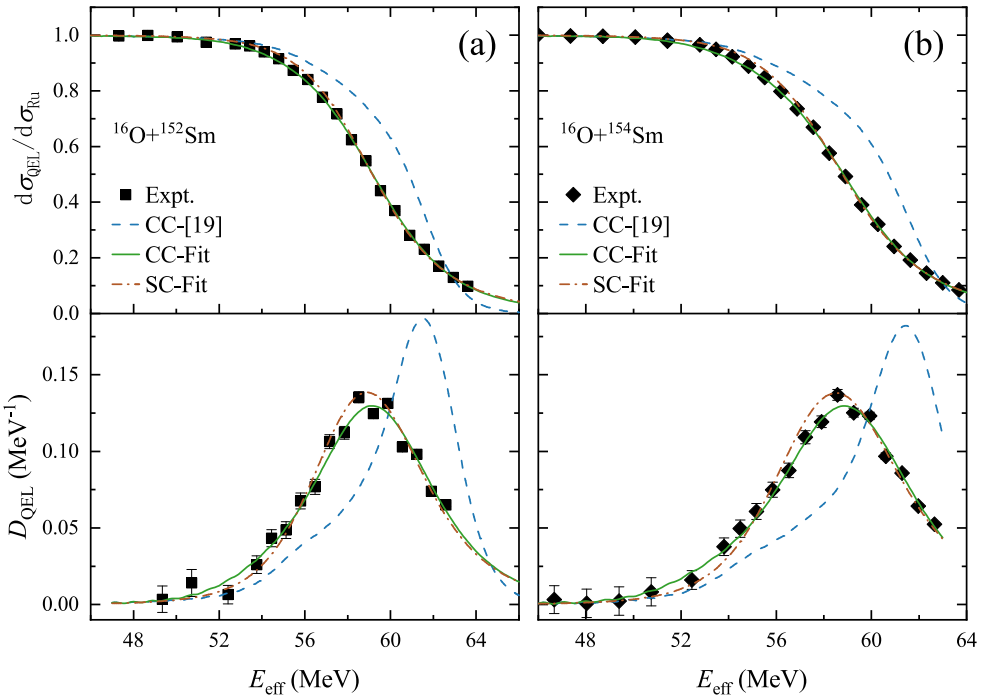

Fig. 1. (color online) Comparison of the experimental data with the fit results using the CC and SC calculations of the ^{16}O +^{152,154}Sm systems and the calculation using the short-range imaginary-part potential in Ref. [19]. The dashed line is the calculation using the potential in Ref. [19], the solid and dash-dot-dotted lines are the calculations using the CC and SC fit results, respectively.

Table 3. Best imaginary parameters W, r_W, and a_W extracted from the CC and SC calculations, together with χ^2 per degree of freedom of the best fit.

System	Method	W/MeV	r_W/fm	a_W/fm	$\chi^2_{\min}/\nu$
^{16}O+^{152}Sm	CC	5.927 ± 0.707	1.495 ± 0.005	0.147 ± 0.011	2.37
	SC	115.52 ± 31.29	1.308 ± 0.009	0.317 ± 0.009	5.46
^{16}O+^{154}Sm	CC	4.566 ± 0.218	1.525 ± 0.004	0.058 ± 0.012	1.44
	SC	91.84 ± 21.49	1.325 ± 0.008	0.319 ± 0.008	4.17
^{16}O+^{184}W	CC	5.703 ± 0.343	1.508 ± 0.004	0.011 ± 0.001	0.87
	SC	48.35 ± 20.47	1.415 ± 0.007	0.219 ± 0.007	3.10
^{16}O+^{186}W	CC	6.107 ± 0.388	1.509 ± 0.004	0.064 ± 0.013	0.98
	SC	60.44 ± 28.24	1.402 ± 0.010	0.236 ± 0.008	4.47

meters and real-part nuclear potential. The results obtained with the short-range imaginary-part potential (dashed line) in Ref. [19] have deviated from the experimental data in the energy region near the Coulomb barrier, and the peak position of the barrier distribution has shifted to the high-energy region.

The specific values are shown in Table 3. The fit resultsfor both Sm and W are shallow long-range imaginary-part potentials. The contrary sign of β_4 for Sm and W does not introduce an obvious difference for the imaginary potential.

B. Parameters results and errors

The imaginary-part parameters W, r_W, and a_W obtained from the best fits, with and without couplings, are summarized in Table 3. The uncertainties in the imaginary-part potential parameter were calculated according to the following procedure [37]. Using the χ^2 minimum value ($\chi^2_{\min}$) corresponding to the best-fit value of the imaginary-part parameters, the quantity

$$\hat{\chi}^2/\nu = \chi^2_{\min}/\nu + \mathrm{UP} \tag{25}$$

was calculated, where UP = 3.53 for the three-parameter fit [37], and ν denotes the number of degrees of freedom. In the cases where χ^2/ν exceeded 1.5, the uncertainties on W, r_W, and a_W were multiplied by $\sqrt{\chi^2_{\min}/\nu}$ [14].

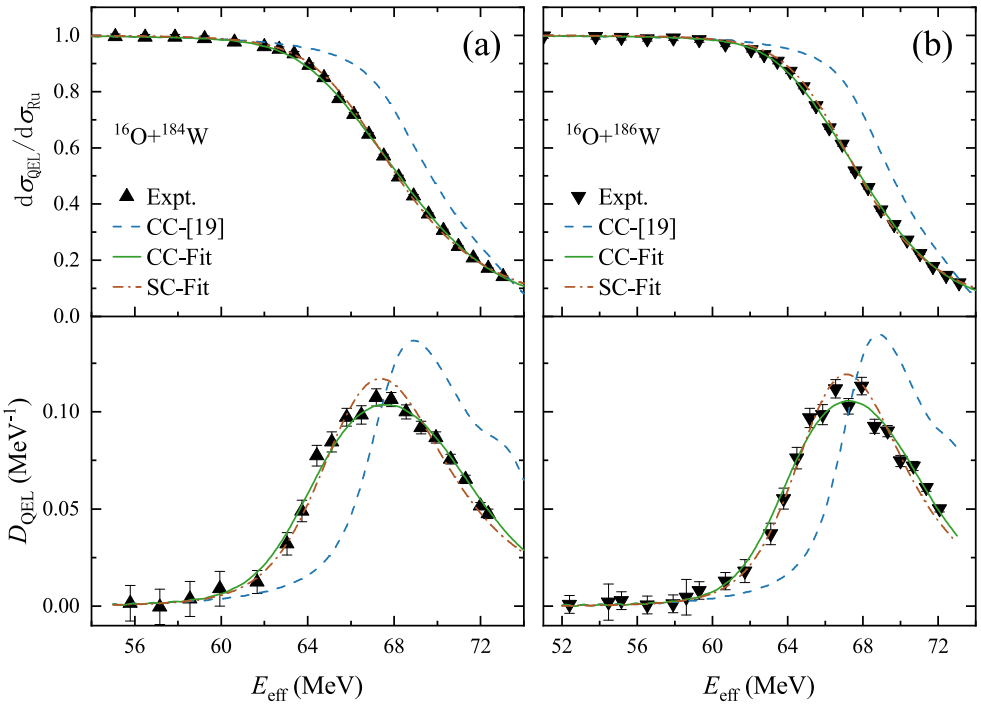

Fig. 2. (color online) The same as Figure 1 but for ^{16}O+^{184,186}W reactions.

Table 3 shows that SC fittings to the quasi-elastic scattering data give large imaginary-part potential depth errors up to 30 MeV, while coupled-channels analyses lead to values for W in the narrower range of the errors less than 1 MeV. Taking ^{16}O+^{152}Sm as an example, the variation of the SC calculation results with varied W within its error are shown in Fig. 3 by the shadow grey area, with the fixed imaginary-part potential parameters r_W and a_W. The SC-calculation result is insensitive to the depth of the imaginary-part potential.

A comparison of the fitted potentials and potential used in Ref. [19] for ^{16}O+^{186}W is shown in Fig. 4. According to Fig. 4, the imaginary-part potentials obtained by both the SC and CC fit are longer-range than that used in Ref. [19]. The imaginary potential of CC extracted in the present work is different from that of SC. The imaginary potential extracted by CC is shallower and longer-range, and the coupling-channel effect shows absorption, which corresponds to the enhancement of fusion cross sections below the barrier [21].

Love *et al.* [38] proposed that the strong coupling effect may also be explained in terms of a long-range predominantly imaginary dynamic polarisation potential (DPP) induced by the Coulomb coupling which, when added to a conventional optical-model potential, provided a good description of the ^{18}O+^{184}W elastic-scattering experimental angular-distribution data at 90 MeV. For deformed nuclei, long-range DPPs arise from the effect of the long-range Coulomb excitation of a rotational band, which is performed by a strongly depleted elastic-scattering cross section [39, 35]. This also corresponds to the

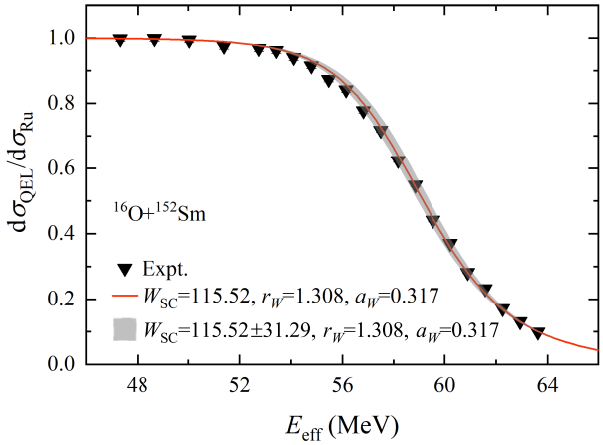

Fig. 3. (color online) Comparison of the experimental data and SC calculation for ^{16}O+^{152}Sm. The solid line and shadow gray area are the SC calculations using the best-fit result of W and its confidence level (1σ).

long-range imaginary-part potential obtained in this work.

Because deformation is emphasized during fitting, a critical advantage of the extracted long-range imaginary potential lies in its ability to provide the possibility to extract deformation parameters across the whole energy range (sub- to above-barrier regions). The traditional short-range imaginary potential [19] is limited to the low-energy region, where the Coulomb interaction is stronger and more sensitive to Coulomb deformation. In a previous work [22], the Coulomb deformation is typically treated as the same as the nuclear deformation. However, the Coulomb deformation is slightly larger than the nuc-

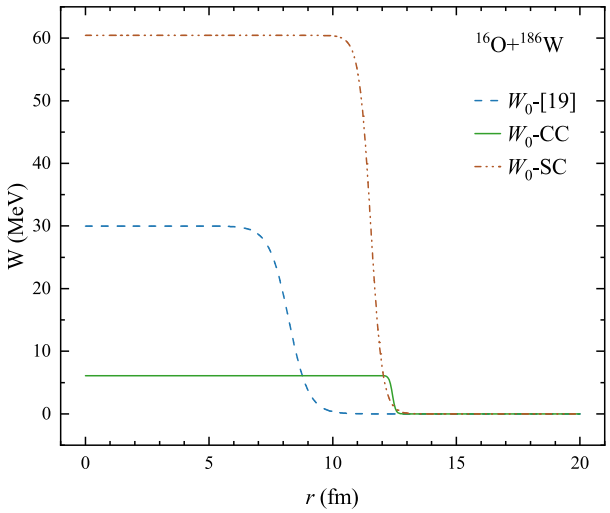

Fig. 4. (color online) Comparison of our fitted potentials and the potential used in Ref. [19] for ^{16}O+^{186}W. The dashed line is the potential used in Ref. [19], and the solid and dash-dot-dotted lines are the fitted potential using the CC and SC fit result, respectively.

lear deformation. Reproducing the backangle quasi-elastic excitation function over the whole energy region by the long-range imaginary-part potential will help to extract the deformation parameters over the whole energy region, and can more realistically reflect the deformation of the nuclear-material distribution. The systematic analysis of more deformed systems to obtain an appropriate imaginary-part potential still needs to be addressed, and the present work is only a preliminary attempt. It may provide a method to extract the deformation parameters for heavier systems through the appropriate choice of the imaginary potential.

IV. SUMMARY AND CONCLUSIONS

The imaginary-part potential parameters were extracted from the quasi-elastic scattering of ^{16}O +^{152,154}Sm, ^{184,186}W using CC and SC calculations. A long-range imaginary potential for the systems with well-deformed nuclei is needed for describing the experimental quasi-elastic scattering excitation-function data in the near-barrier energy region using CC calculations. Compared to the short-range imaginary-part potential used in Ref. [19] for the sub-barrier data, the present results show that a long-range imaginary-part potential is needed for backward quasi-elastic scattering at a wide energy region covering the Coulomb barrier. Considering the deformation effect, the long-range imaginary-part potential obtained here reflects the strong absorption effect of the large deformation systems. In previous works, only a few attempts [40−43] have been made to reproduce elastic scattering and fusion experimental data simultaneously using the same potential. This finding is helpful to bridge the gap between fusion and scattering descriptions for well-deformed systems. Further systematic and more detailed studies with different projectile-target combinations from light to heavy systems are needed.

References

[1] J. Cook, At. Data Nucl. Data Tables **26**, 19 (1981)
[2] M.E. Brandan and G.R. Satchler, Phys. Rep. **285**, 143 (1997)
[3] F.D. Becchetti, P.R. Christensen, V.I. Manko *et al.*, Nucl. Phys. A **203**, 1 (1973)
[4] C. J. Lin, J. C. Xu, H. Q. Zhang *et al.*, Phys. Rev. C **63**, 064606 (2001)
[5] George Igo, Phys. Rev. Lett. **1**, 72 (1958)
[6] G.R. Satchler and W.G. Love, Phys. Rep. **55**, 183 (1979)
[7] Aage Winther, Nucl. Phys. A **594**, 203 (1995)
[8] Ishwar Dutt and Rajeev K. Puri, Phys. Rev. C **81**, 064609 (2010)
[9] T. Furumoto, Y. Sakuragi, and Y. Yamamoto, Phys. Rev. C **78**, 044610 (2008)
[10] L. Yang, C. J. Lin, H. M. Jia *et al.*, Phys. Rev. Lett. **119**, 042503 (2017)
[11] C. J. Lin, L. Yang, H. M Jia *et al.*, PoS **281**, 203 (2017)
[12] A. B. Balantekin, S. E. Koonin, and J. W. Negele, Phys. Rev. C **28**, 1565 (1983)
[13] J.O. Newton, R.D. Butt, M. Dasgupta *et al.*, Phys. Lett. B **586**, 219 (2004)
[14] J. O. Newton, R. D. Butt, M. Dasgupta *et al.*, Phys. Rev. C **70**, 024605 (2004)
[15] C. J. Lin, H. M. Jia, H. Q. Zhang *et al.*, Phys. Rev. C **79**, 064603 (2009)
[16] P.R. Christensen and Z.E. Switkowski, Nucl. Phys. A **280**, 205 (1977)
[17] A. Mukherjee, D. J. Hinde, M. Dasgupta *et al.*, Phys. Rev. C **75**, 044608 (2007)
[18] M. L. Inche Ibrahim, Muhammad Zamrun, and Hasan Abu Kassim, Phys. Rev. C **87**, 024611 (2013)
[19] K. Hagino and N. Rowley, Phys. Rev. C **69**, 054610 (2004)
[20] K. Hagino, T. Takehi, A. B. Balantekin *et al.*, Phys. Rev. C **71**, 044612 (2005)
[21] J. R. Leigh, M. Dasgupta, D. J. Hinde *et al.*, Phys. Rev. C **52**, 3151 (1995)
[22] H. M. Jia, C. J. Lin, F. Yang *et al.*, Phys. Rev. C **90**, 031601 (2014)
[23] H. Timmers, J.R. Leigh, M. Dasgupta *et al.*, Nucl. Phys. A **584**, 190 (1995)
[24] K Hagino, N Rowley, and AT Kruppa, Comput. Phys. Commun. **123**, 143 (1999)
[25] K. Hagino and N. Takigawa, Prog. Theor. Phys. **128**, 1061 (2012)
[26] P. Descouvemont, Comput. Phys. Commun **200**, 199 (2016)
[27] A. B. Balantekin and N. Takigawa, Rev. Mod. Phys. **70**, 77 (1998)
[28] H. Esbensen, S. Landowne, and C. Price, Phys. Rev. C **36**, 2359 (1987)
[29] E. Piasecki, M. Kowalczyk, K. Piasecki *et al.*, Phys. Rev. C

65, 054611 (2002)
[30] P. Möller, A.J. Sierk, T. Ichikawa *et al*., At. Data Nucl. Data Tables **109-110**, 1 (2016)
[31] National Nuclear Data Center. https://www.nndc.bnl.gov/nudat3/.
[32] F. James and M. Roos, Comput. Phys. Commun. **10**, 343 (1975)
[33] Rainer Storn and Kenneth Price, J Global Optim. **11**, 341 (1997)
[34] T. Izumoto, T. Udagawa, and B. T. Kim, Phys. Rev. C **51**, 761 (1995)
[35] R. G. Stokstad and E. E. Gross, Phys. Rev. C **23**, 281 (1981)
[36] Byung-Taik Kim, Phys. Lett. B **80**, 353 (1979)
[37] Peter McCullagh. *Generalized Linear Models* (2nd edition, Boca Raton: Chapman and Hall/CRC, 1989)
[38] W.G. Love, T. Terasawa, and G.R. Satchler, Nucl. Phys. A **291**, 183 (1977)
[39] C. E. Thorn, M. J. LeVine, J. J. Kolata *et al*., Phys. Rev. Lett. **38**, 384 (1977)
[40] S. E. Vigdor, D. G. Kovar, P. Sperr *et al*., Phys. Rev. C **20**, 2147 (1979)
[41] M Hugi, L Jarczyk, B Kamys *et al*., J Phys. G: Nucl. Partic. **6**, 1257 (1980)
[42] S. Kailas and S. K. Gupta, Phys. Rev. C **34**, 357 (1986)
[43] H. Esbensen, C. L. Jiang, and K. E. Rehm, Phys. Rev. C **57**, 2401 (1998)